RSC Advances

ROYAL SOCIETY OF CHEMISTRY

www.rsc.org/advances

ARTICLE TYPE www. rsc.org/xxxxxx | XXXXXXXX

Single-walled carbon nanotube composite inks for printed gas sensors: Enhanced detection of NO_2, NH_3, EtOH and Acetone

Gwyn P. Evans[a], David J. Buckley[b], Neal T. Skipper [b] and Ivan P. Parkin[c]

Received xxxx xxxxxxx 20xx, Accepted xxxx xxxxxxxx 20xx
First published on the web Xth XXXXXXXXXX 200X
DOI: 10.1039/b000000x

The monitoring and detection of harmful vapours and precursor gases is an ever present concern to security services, industry and environmental groups. Recent advances in carbon nanotube based resistive sensors highlight potential applications in explosive detection, industrial and environmental monitoring. Metal oxide semiconducting (MOS) gas sensor technology also shows promise when applied in discriminatory arrays to form an electronic nose. Novel single-walled nanotube (SWNT) - metal oxide (SnO_2 and WO_3) composite inks were synthesised and used to fabricate sensors with enhanced responses to low concentrations of NO_2, NH_3, acetone and EtOH vapours. Characterisation of the sensing material was accomplished by X-ray diffraction (XRD), Raman spectroscopy, thermo-gravemetric analysis (TGA), UV-Vis-IR absorption spectroscopy (UV-Vis-IR), transmission electron microscopy (TEM) and scanning electron microscopy (SEM). The enhancements were found to depend on the preparation route and operating temperature of the devices. A micro-structural model of resistance contribution was applied to explain the improvements of up to 198% in sensor response. Modification of sensing characteristics, through incorporation of SWNTs produced by the high pressure carbon monoxide disproportionation (HiPco) process, provides a new route to improved sensitivity and selectivity in an array of SWNT modified devices, useful in trace gas detection.

1 Introduction

The detection and monitoring of precursor gases is a vital requirement in many industrial processes[1], environmental safety[2] and security applications[3]. Such instances include the regulation of NH_3 in agricultural production[4], the monitoring of CO_2 and ozone levels to gauge air pollution[5], and the detection of illicit substances[6]. There exists a wide range of technologies currently employed to achieve trace detection of target gases and vapours such as electrochemical sensors, ion mobility mass spectrometry, and trained sniffer dogs[7]. However, the need for more affordable, portable, sensitive and rapid trace detection techniques remains.

The use of single-walled carbon nanotube (SWNT) based sensors to detect oxidising and reducing gases in ambient environmental conditions, has attracted considerable research interest in recent years. Such devices are sensitive to a wide range of vapours and can operate at room temperature[8–11]. Functionalisation of the different types of SWNTs permits selective detection to low concentrations[12]. Undesirably, reported response magnitudes ($|S|$) to target gases are comparatively low[13] (e.g $|S|$ to 100 ppm $NO_2 \approx 4$) to those achieved with established metal oxide semiconducting (MOS) gas sensor technology[6] (e.g $|S|$ to 0.35 ppm $NO_2 \approx 23$), along with the observation of extended sensor recovery times[14].

Commercially produced MOS gas sensors meet many of these aforementioned criteria, but require a high operating temperature[15] (200 °C to 450 °C) limiting applications, whilst also lacking selectivity to specific gases. Studies have shown that the addition of materials such as zeolites[16–18] and nanostructures[19] to MOS gas sensors can increase sensor responses, thus improving the selectivity achievable in a sensory array or e-nose.

In an effort to develop a sensor that combines the preferential qualities of each sensor type, much work has concentrated on the decoration of SWNTs with metal oxide nanoparticles to achieve measurable changes in the conductivity of the material upon the introduction of a target gas to the sensing device at room temperature[20–22]. The fabrication of metal oxide modified SWNT materials has been reported via electrochemical techniques, the sol-gel process and gas phase deposition[23,24]. Multi-walled carbon nanotube (MWNT)-metal oxide composites have also been used in gas sensing applications[25].

However, there is little reported research on the responses of SWNT-metal oxide composite gas sensors to target gases and vapours that are operated at higher temperatures (250 °C

[a] *Dept. of Security and Crime Science, University College London, 35 Tavistock Sq., London, WC1H 9EZ, UK*
[b] *London Centre for Nanotechnology and Department of Physics and Astronomy, University College London, Gower Street, London WC1E 6BT, U.K.*
[c] *Dept. of Chemistry, University College London, 20 Gordon St., London, WC1H 0AJ, UK, E-mail: i.p.parkin@ucl.ac.uk; Fax: +44 (0)20 7679 7463; Tel: +44 (0)20 7679 4669*
† Electronic Supplementary Information (ESI) available:See DOI: 10.1039/b000000x/

350 °C). Furthermore, there have been few studies on the incorporation of SWNTs with metal oxide based inks, suitable for deposition via the commercially scalable screen printing method.

In this work, SWNTs produced via the high pressure carbon monoxide disproportionation (HiPco)[26,27] process are incorporated with SnO_2 and WO_3 metal oxide powders to form novel HiPco SWNT-metal oxide inks, via a facile synthesisation process. The inks were subsequently used to fabricate an array of SWNT-metal oxide composite resistive gas sensors, which were tested against their unmodified metal oxide counterparts to oxidising and reducing gases. Enhancements in sensor responses to NO_2, NH_3, EtOH and Acetone were observed at low vapour concentrations. These enhancements were found to be dependent upon composite preparation route and device operating temperature.

2 Experimental Section

2.1 SWNT Preparation

SWNTs produced via the HiPco process[26,27] were purchased from nanointegris (batch number: R1-831). The black powder was dried in air at 120 °C to remove moisture from the characteristic SWNT bundles and stored under vacuum. The following surfactant wrapping was then performed in air at room temperature.

The tubes were first dispersed in a solution of sodium deoxycholate and heavy water (DOC D_2O) at a concentration of approximately 0.5 $mgml^{-1}$. The container was placed in a propanol bath and the solution sonicated using a 225W tip sonication probe 15 minutes. The DOC D_2O forms micelle like structures around the tubes[28], reducing re-aggregation of the SWNT to bundles, aiding an efficient solubilisation and individualisation.

Before the SWNTs underwent subsequent characterisation studies or material synthesisation, they were centrifuged at 4000 g for 30 minutes. The upper 80% of the final solution was then decanted to limit the presence of impurities and bundles which inhibit optical characterisation. The DOC D_2O tip sonication process introduces defects to the solution as reported by Zhang et al[29].

2.2 SWNT-Metal Oxide Ink

An organic texanol based vehicle (ESL-400, Agmet Ltd) was mixed with SnO_2 and WO_3 commercial powders (Sigma-Aldrich). The surfactant wrapped tubes were then added to the metal oxide ink (1 wt%). A pestle and mortar was used to grind the ink into a homogeneous mixture for 10 minutes.

The TGA data confirms the removal of the DOC D_2O solution and the ESL-400 vehicle from the sensing material. The resulting sensor composite is of polycrystalline metal oxide structure with SWNT bundles embedded within the material. Finally, the device is attached to the sensor casing via micro welded platinum wire connections to the gold electrodes and platinum heater track.

2.3 Device Fabrication

The produced SWNT-metal oxide based inks were screen printed (4 x layers) using a DEK1202 commercial screen printer onto 3 x 3 mm alumina substrates, interdigitated with gold electrodes (Fig. 1a). A platinum heater track is located on the underside of the sensor substrate to bring the device to operating temperature during testing (Fig. 1b).

These were subsequently annealed in air to 400 °C to remove the ESL-400 vehicle and aid adherence of the composite material to the substrate. The final array of sensors is detailed in Table 1

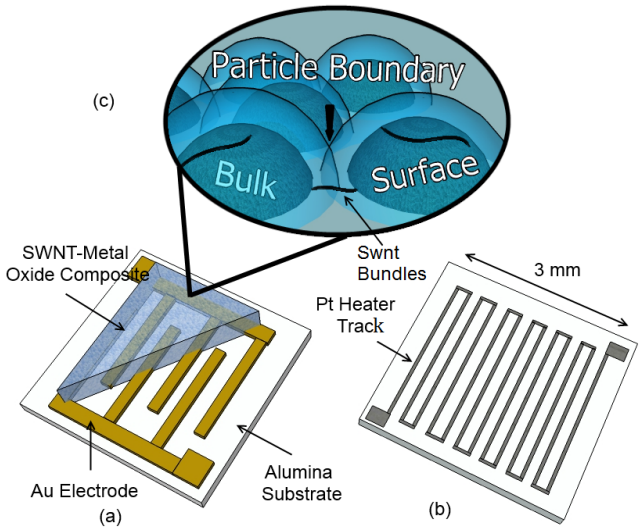

Fig. 1 A schematic diagram of the 3 x 3 mm interdigitated alumina substrate with (a) gold electrodes and screen printed material, (b) platinum heater track located on the reverse. The components of the simple model for micro-structural resistance contribution (c) within the composite material are also shown

2.4 Gas Testing Procedure

The sensors were tested to target gases as detailed in Table 2. During each testing cycle a program was used in conjunction with mass flow controllers to adjust the concentrations present in the testing chamber.

Sensors were operated in air for 1200 seconds to establish the baseline resistance of the material. Increasing concentrations of the target vapour were then introduced for a pulse

Table 1 Sensor material, annealing temperature during fabrication and the sensor baseline resistance in air whilst operating at 250 °C

Sensor Material	Annealing Temperature (°C)	Baseline resistance in air (MΩ)
SnO_2 + Swnt	400	21
SnO_2	400	0.18
SnO_2	600	0.06
WO_3 + Swnt	400	5.8
WO_3	400	0.026

length of 600 seconds, followed by a purge cycle in air for 800 seconds.

The response magnitude of the n-type material to a reducing gas such as NH_3 was calculated as the ratio of the baseline resistance in air to the measured resistance across the sensing material (R_0 / R). For oxidising gases such as NO_2, the magnitude was calculated as (R / R_0).

The testing rig has been described previously[6]. Each test was repeated to ensure consistency in the recorded responses. Differences in these repeated experiments were taken as the uncertainty on electrical response to the target gases, as indicated by Fig.S13.

2.5 Characterisations

Characterisation techniques were used to confirm the presence of SWNTs on the sensor surface, in the bulk of the composite and to detect micro-structural changes in the metal oxides after the fabrication process and gas testing.

Raman spectroscopy was performed using a Renshaw Raman microscope spectrometer with laser wavelength 488 nm and 1 mW power. To obtain the Raman spectra for the initial solution, the surfactant wrapped SWNTs were deposited onto a glass substrate and dried in air for 1 hour. The Raman spectra of the final sensing composite was acquired after screen printing the material onto the sensor substrate.

Scanning electron microscopy (SEM) data was obtained using a Jeol JSM-6301F microscope in secondary electron imaging mode, using a 10kV probe voltage.

Transmission electron microscopy (TEM) was performed using a Jeol 200kV transmission electron microscope in imaging mode for the SWNT-metal oxide inks. The inks were drop coated onto a carbon coated copper TEM grid purchased from Agar Scientific. A Jeol 100kV transmission electron microscope was used to image the SWNT-metal oxide composite material after sensor fabrication and post gas testing. The sensing layer was removed from the device, dispersed in hexane via sonication for 5 minutes and subsequently dropped onto a holey carbon coated copper TEM grid (Agar Scientific).

The UV-Vis-IR absorption spectra were taken using a Perkin Elmer Lamda 950 spectrometer for the initial SWNT solution. The background measurements for the D_2O DOC have been subtracted.

X-ray diffraction studies were performed using a Panalytical XPert θ-θ powder diffractometer over the 2θ range 20 ° to 70^o, at a step size of 0.02^o with a copper x-ray source (λ = 0.15419 nm). TGA profiles were obtained using a Netsch TA45 DSC/TGA, to a temperature of 800 °C, with a ramp rate of 15 °C per minute.

3 Results and Discussion

SWNT composite inks were deposited via the repeatable and commercially scalable screen printing method to produce the final sensing device. The modified sensor type, chosen target gases and the response enhancements observed in comparison with non modified sensors are detailed in Table 2. Material characterisations were performed pre and post device fabrication and throughout gas sensor testing process.

Table 2 Modified sensor type, target gases and response enhancement per gas at maximum concentration whilst operating at a temperature of 250 °C

Sensor Type	Target Gas	Response Enhancement (%)
SnO_2 + HiPco SWNT	Acetone, NH_3	72, 198
	EtOH, NO_2	12, 95
WO_3 + HiPco SWNT	NO_2, EtOH	51, 75

3.1 Material Characterisation

The presence of SWNTs in the initial SWNT solution and on the surface of the SWNT-metal oxide composite material pre and post annealing to 400 °C was confirmed by Raman spectroscopy (Fig.2 and Fig.3).

The spectrum of the final device shows the characteristic SnO_2 peaks, as well as the radial breathing modes (RBM) in the range 150 to 300 cm^{-1}, unique to carbon nanotubes. The position and intensity of these peaks is dependent on the diameter of the tubes present and thus specific SWNT chiralities[30].

The G-band splitting is consistent with a sample containing metallic and semiconducting SWNT as is expected for HiPco produced nanotubes[31]. The ratio of the D peak (at

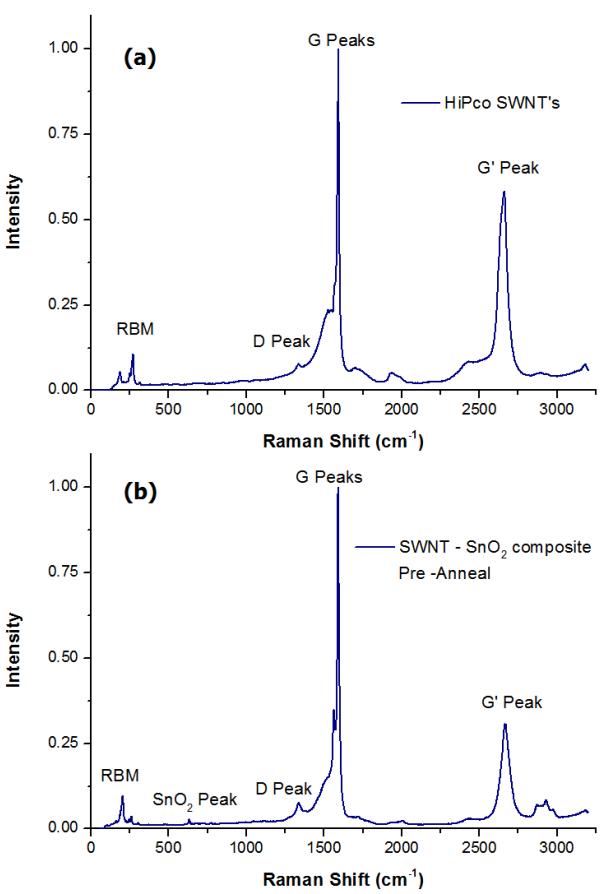

Fig. 2 Raman spectra of (a) HiPco single-walled nanotubes wrapped in a solution of sodium deoxycholate (DOC) and heavy water (D_2O) and dried upon a glass substrate, (b) SWNT-SnO_2 composite in printed form on the sensor substrate pre annealing (λ = 488 nm).

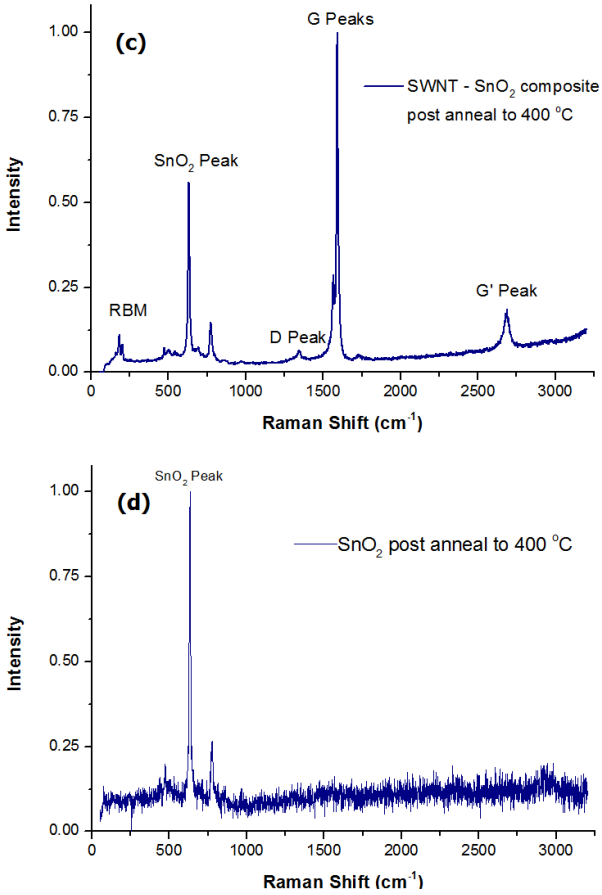

Fig. 3 Raman spectra of (c) SWNT-SnO_2 composite in printed form on the sensor substrate post annealing at 400 °C and (d) blank -SnO_2 on sensor substrate (λ = 488 nm).

1336 cm^{-1}) to the G peak (at 1592 cm^{-1}) shows a low number of defects and amorphous carbon[32] present in the initial solution and final sample (D / G = 0.07).

Transmission electron microscopy was used to qualitatively analyse the dispersion of HiPco SWNTs throughout the metal oxide inks.

Despite surfactant wrapping of the HiPco SWNTs, Fig. 4a shows significant bundling of tubular networks. This may be due to an increase in surface tension between individually wrapped tubes during the drying process, causing re-aggregation. Bundles of between 10 and 30 SWNTs were often found to interconnect between the metal oxide particulates present in the sample (Fig. 4b and Fig. 4c).

The fainter dark patches contained within the tubular bundles shown in Fig. 4d, are identified as residual iron impurities from the HiPco process[33]. Profile analysis of the images yield a mean tube diameter of 0.88 nm, within the expected range for tubes produced via the HiPco process[34] .

TEM was also performed on the SWNT metal oxide composite upon completion of gas testing. After annealing and testing to target vapours, the frequency of interconnecting SWNTs and metal oxide particles was reduced but still visible, as shown in Fig.4. Visual comparison between TEM images of the final composite material and the initial composite ink indicates that the fabrication process and testing produces an increase in deformity and impurities within the tubular bundles.

Surface imaging of the plain metal oxide sensors by SEM demonstrates the porous nature of the metal oxide material (Fig. 5e and Fig. 5f). A porous material increases accessibility of the gas to resistive components of the material micro-structure[35].

A micrograph of the initial SWNT solution drop deposited to form a dry film (Fig. 5b) shows the tendency of SWNT bundles to bridge cracks in the film surface.

TGA profiles were primarily used to determine a sufficient

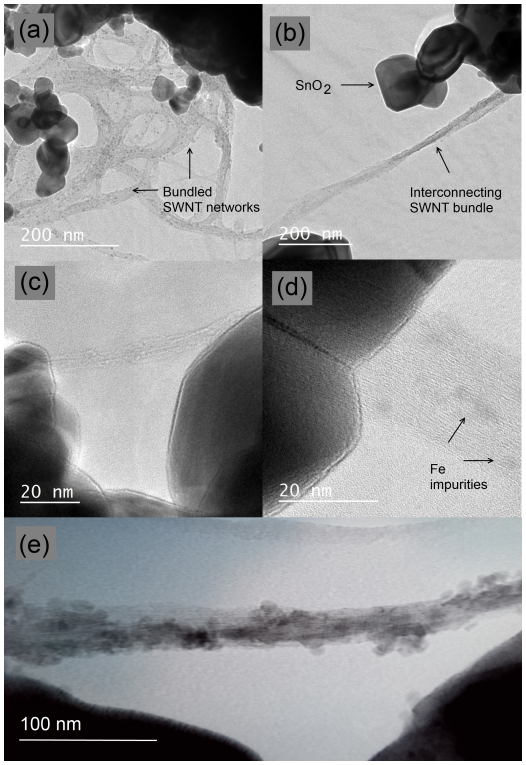

Fig. 4 Images taken using a Jeol 200kV transmission electron microscope in imaging mode showing (a) dispersion of HiPco SWNT bundles containing Fe impurities amongst larger SnO_2 particles 20,000x (b) interconnectivity of SnO_2 particles 25,000x (c) particle bridging 80,000x (d) SWNT bundle diameters 200,000x (e) nanotube bundle post fabrication and testing in SWNT-SnO_2 composite

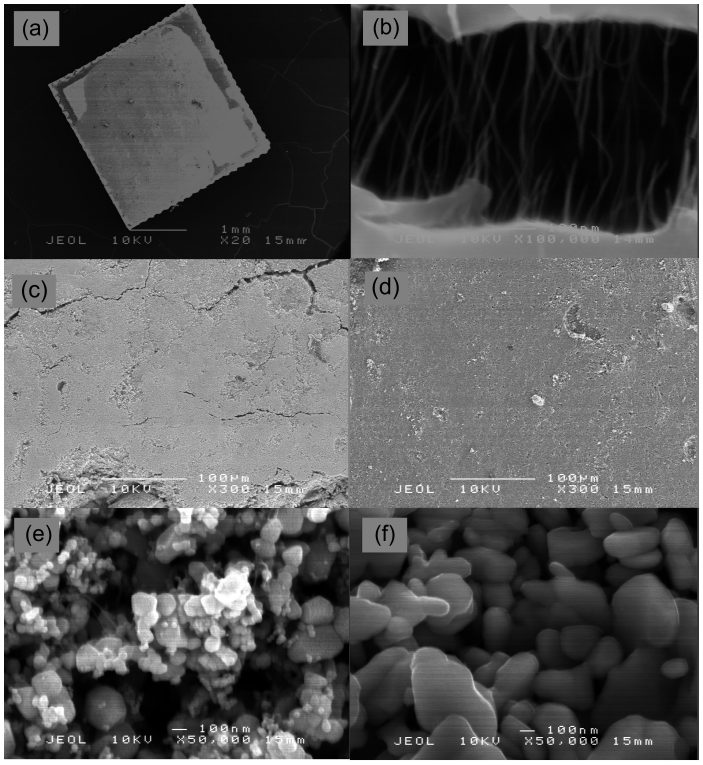

Fig. 5 SEM micrographs of SnO_2 and WO_3 blank sensors on interdigitated alumina substrate at varying magnifications and a dried solution of HiPco SWNT bundles (a) SnO2 20x (b) Deposited Initial SWNT Solution 100000x (c) SnO2 300x (d) WO3 300x (e) SnO2 50,000x (f) WO3 50,000x

annealing temperature to remove residual solvent and surfactant. Annealing is also required to ensure polycrystalline structure throughout the metal oxide, important in achieving a good sensor response[36], and aid stability whilst operating the devices at elevated temperatures[37]. TGA data is available in the supplementary information provided. The ESL vehicle is removed from the material at 400 °C, with a ramp rate of 15 °C per minute. Removal of the surfactant used to wrap the SWNTs takes place at 200 °C. The HiPco SWNTs were found to decompose between 400 °C and 500 °C at a ramp rate of 5 °C per minute.

XRD spectra were taken pre and post testing to provide an indication of any structural changes (Fig.S11 and Fig.S12). Diffraction peaks are labelled with reference to those reported in the literature[38,39]. X-ray diffraction scans were collected over the $2(\theta)$ range 20^o to 70^o at a step size of 0.02^o with a copper X-ray source (λ=0.15419nm). The crystallite sizes of the metal oxide powders were found to be approximately 70 nm, remaining constant pre and post testing. The method used to estimate crystallite size is detailed in the supplementary information.

The UV-Vis-IR absorption spectra for the initial SWNT solution (diluted to 0.003 $mgml^{-}1$) is shown in Fig.6. Optical adsorption bands for SWNTs are related to allowed transitions between van Hove singularities in the valence and the conductive bands of the nanotube electronic density of states (DOS)[40]. These diameter dependent singularities appear due to the 1-D nature of nanotube electronic structure[40]. A range of metallic and semiconducting tubes are present in the sample[41] as shown in Fig.6, where E_{ii} denotes transitions between the indexed valance and conduction bands.

The range of peaks correspond to specific SWNT chiralities and diameters[27,42]. Using the Kataura plot for SWNTs in aqueous suspension proposed by Weisman et al[43], the range of tube diameters present in the sample can be estimated as 0.8nm to 1.2 nm.

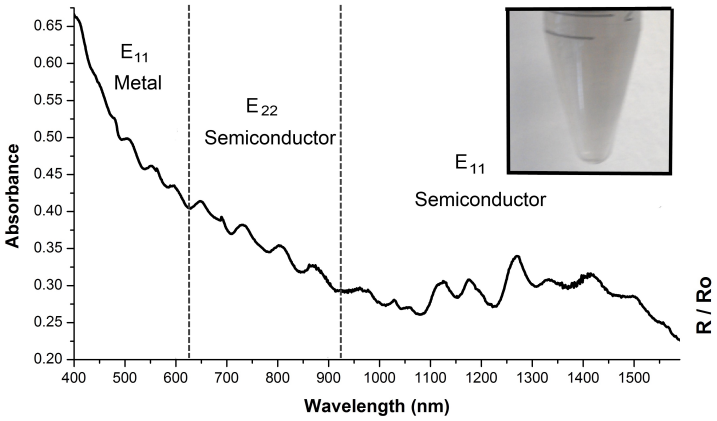

Fig. 6 UV-Vis-IR absorption spectra, displaying the range of metallic and semiconducting tube species present in the initial SWNT solution (diluted to 0.003 mgml^{-1} as in image displayed)

3.2 Gas Testing

Absorption or desorption of a gas on the surface of a metal oxide produces a change in conductivity when a potential difference is applied across the material [15]. This is dependent on electrons having enough energy to cross from the valence to the conduction band [2]. MOS gas sensors supply this required energy via heat transfer from a heating element. In this case the Pt heater track is located on the reverse of the sensor substrate (Fig. 1b).

The metal oxides used in sensor fabrication were chosen on the basis of known sensitivities to the target vapours. WO_3 reportedly provides a large response to the oxidising gas NO_2 [1], whilst SnO_2 was chosen for it's sensitivity to the reducing gases NH_3, EtOH and acetone [44].

Both metal oxides are n-type semiconductors and are used in commercially produced gas sensors. N-type materials display an increase in resistance when exposed to oxidising vapours and a resistance decrease when exposed to reducing vapours [15]. Conversely, the incorporated HiPco SWNTs are p-type, displaying a decrease in resistance to oxidising gases and an increase to reducing gases [13]. The chosen metal oxides and the SWNT modified devices were tested to the aforementioned gases to investigate the changes in sensing characteristics displayed by the composite material.

3.3 Sensitivity Enhancement

An increase in response magnitude for SWNT modified sensors was observed to all target gases whilst operating at the lower temperature of 250 °C. Fig.7 exhibits an enhancement of 77% when testing on NO_2 using a SWNT - WO_3 modified material at 200 ppb. This enhancement was consistently observed through a range of low vapour concentrations.

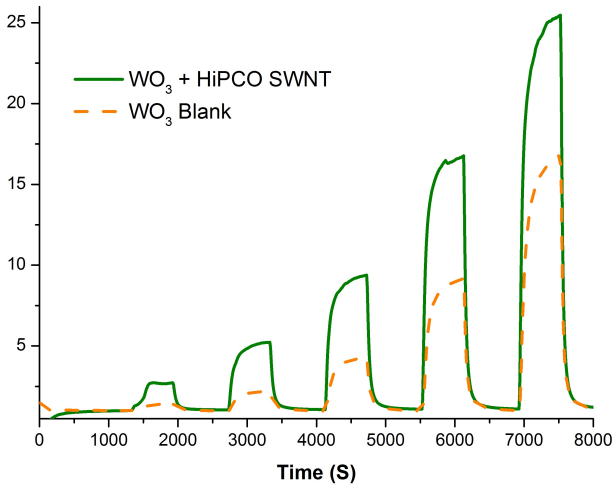

Fig. 7 WO_3 Blank and SWNT - WO_3 composite sensor responses to NO_2 at an operating temperature of 250 °C. Testing was to increasing gas concentrations of 50, 100, 200, 400 and 600 ppb

A similar improvement to sensing response is observed when testing on Acetone using an SWNT - SnO_2 modified device at a concentration of 8 ppm. A small drift in baseline resistance is observed (Fig.8). This is not attributed to the incorporation of SWNTs, as the drift occurs for both the SWNT modified and blank SnO_2 sensors.

Both SnO_2 and WO_3 based sensors were tested to EtOH and NH_3. An enhancement in sensing response was again observed in SWNT-metal oxide composite sensors in comparison with their plain counterpart. The increase was more pronounced in the SWNT - SnO_2 modified sensor when testing on NH_3 (Fig.9). Interestingly, the enhancement was greater when sensors were exposed to higher gas concentration.

Fig.S15 compares the response magnitudes between the WO_3 and SnO_2 based sensors whilst testing to NO_2 , along with their SWNT modified analogue. Here, the effect of SWNT incorporation on the SnO_2 sensor response was lower (37%) than the WO_3 based sensor (120%) at lower gas concentration (200 ppb). However, this trend was reversed when testing to higher vapour concentration of 800 ppb. The improvement on SnO_2 response was 94%, where as the enhancement in sensitivity for the SWNT - WO_3 composite sensor fell to less than 11%.

The stronger response of SnO_2 based sensors to EtOH than those observed from WO_3 based devices is shown in Fig.10, when operating at a higher temperature of 300 °C.

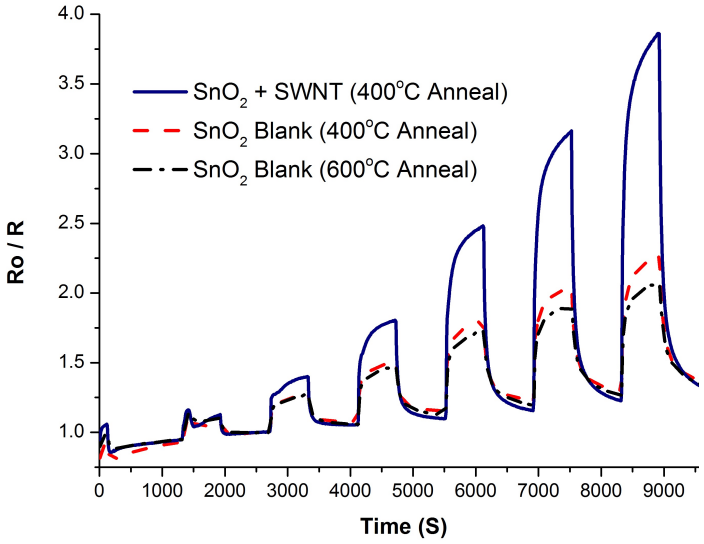

Fig. 8 SnO_2 Blank and SWNT - SnO_2 composite sensor responses to Acetone at an operating temperature of 250 °C. Testing was to increasing gas concentrations of 0.5, 1, 2, 4, 6 and 8 ppm

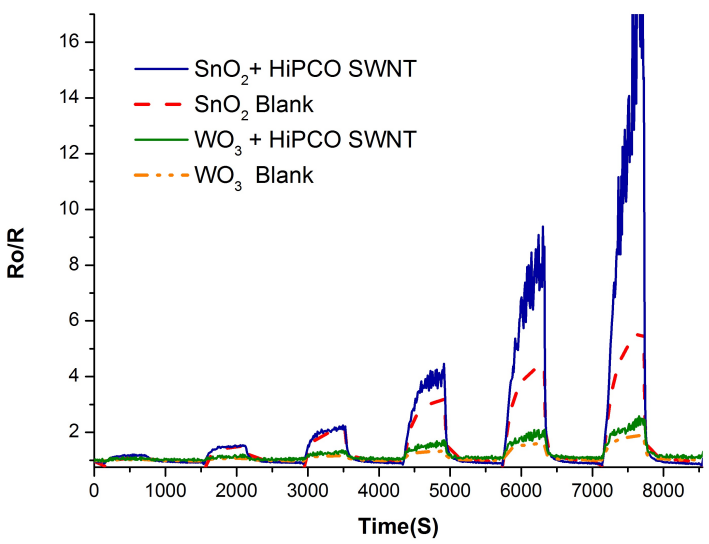

Fig. 9 WO_3 Blank, SWNT - WO_3 composite, SnO_2 Blank and SWNT- SnO_2 composite sensor responses to NH_3 at an operating temperature of 300 °C. Testing was to increasing gas concentrations of 2.5, 5, 10, 20, 30 and 40 ppm

3.4 Temperature and Humidity Dependence

The enhancements achieved when incorporating SWNTs were found to be dependent on the chosen operating temperature of the device. Fig.10a shows how the effects of the SWNT incorporation are reversed when testing to EtOH at a higher operating temperature of 300 °C. The SnO_2 blank sensor exhibits a response larger by 215% than that of the SWNT-SnO_2 composite sensor, when testing to 60 ppm of EtOH vapour. This is also true for the WO_3 blank sensor which displays a response two times larger than it's SWNT analogue when operated at 300 °C.

The operating temperature of entirely SWNT based sensors partially determines device conductivity and thus sensing response[45]. Changes in response upon variation of operating temperature have been reported previously for sensors based purely on carbon nanotubes[46], where a low response of 3% was observed in comparison to those demonstrated by the SWNT-metal oxide inks presented here, whilst testing to 100 ppb of NO_2 and operating at 215 °C.

Testing to Acetone using the SnO_2 based sensors at 300 °C produced a general increase in response, but no significant differences to the SWNT modified sensor were observed when operating at this elevated temperature as detailed in the supplementary information (Fig.S16). For the reducing gases Acetone and EtOH, enhancements to the modified sensors are not observed at higher temperatures.

It has been previously reported that the response of metal oxide sensors operating above 300°C depends on the number of oxygen vacancies available, whilst at lower temperature (<275°C) the response is more dependant on the size and surface area of the material when testing with reducing gases[47]. This may explain the temperature dependant responses seen here, as SWNT inclusion alters both the morphology of the sensing material and potentially the number of oxygen vacancies available at the surface.

The SWNT-SnO_2 composite sensor showed an increase in sensitivity to humidity as displayed in Fig.S14 , consistent with previous studies on SWNT based sensors[13]. The response enhancements to target gases discussed previously are not due to humidity variations, as tests were carried out in synthetic dry air. Humidity effects are often addressed by applying a filter to the sensor for use in practical applications[48]. Alternatively, the SWNT-SnO_2 composite may be useful as a humidity sensor.

3.5 Enhancement Mechanism

The mechanism for gas sensing is complicated and dependent on many factors, such as material type, chemical composition, grain size and micro-structure[35,49–51]. A simple model of the micro-structural resistance contribution considers electron conduction at particle boundaries, bulk and surface regions as

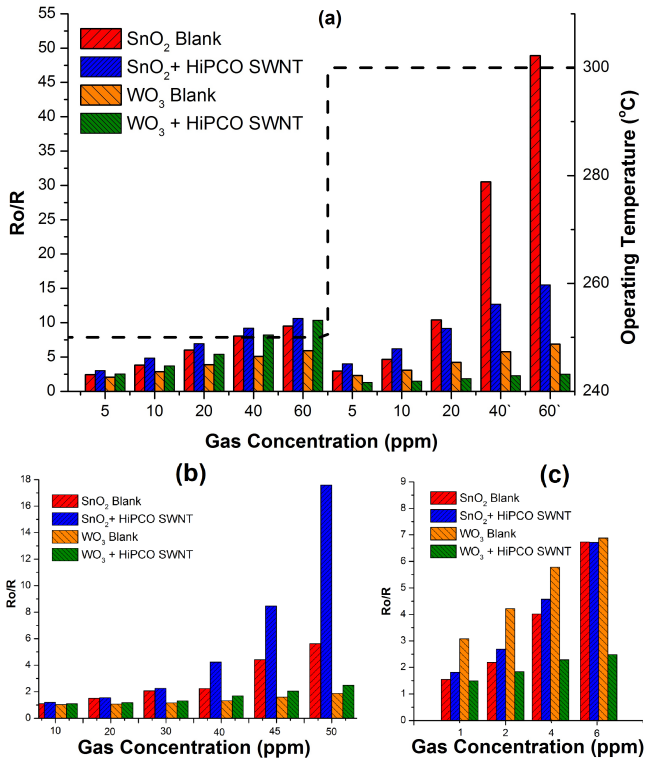

Fig. 10 Differences in response magnitudes between SWNT modified and blank metal oxide sensors to (a) EtOH vapour as a function of gas concentration and operating temperature. (b) NH_3 and (c) Acetone show selectivity as a function of gas concentration operating at 300 °C

described by Williams et al[52]. The degree to which each of these components effects the resistance of a material varies as a function of particle and particle neck size[52]. This model assumes that only the area of a material that is accessible to the introduced gas exhibits a change in resistance. Furthermore, the model is used to relate the response magnitude of a resistive sensor to vapour concentration.

The resistance of an n-type material in air is thought to be dominated by the surface region (defined as a depth equivalent to the Debye length of the material) and at particle boundaries[35]. The introduction of p-type SWNTs at surface and boundary regions may alter sensitivity of the n-type metal oxides to target vapours. This bridging of metal oxide particulates, as observed in Fig.4b, results in p-n boundaries throughout the composite. Such p-n junctions have been previously reported in SWNTs decorated with SnO_2 particles[53], contributing to conductance change in the material.

The presence of SWNTs in these regions gives rise to a large change in resistivity of the material and may explain the large variations in response observed. Table 1 highlights such variations, with the baseline resistances of the SWNT - composite sensors differing by two orders of magnitude when compared with their plain metal oxide counterpart.

The contribution of each resistive component is predicted to vary with gas concentration. This would cause an increase in the difference between a SWNT modified sensor response as a function of vapour concentration, such as that observed in Fig.8 and Fig.9.

Past study of sensing response upon incorporation of MWNT with MOS gas sensors, suggests the presence of tubular nanostructures on the sensor surface increases the reaction area available for charge transfer[54]. TEM image analysis of the SWNT-metal oxide inks produced in the current study, highlights tube bundle formation of similar dimension to the MWNTs used in previous investigations. A similar mechanism (i.e increased charge transfer at the surface) may play a part in the response enhancements observed in the SWNT-metal oxide composite, due to the high dependency of sensing response magnitudes to resistance changes in the surface region as per the model discussed above. An increase in response may be due to the extreme sensitivity of electron conduction in semiconducting SWNTs to the presence of molecules on the tube surface[14].

Thermal treatment of metal oxides in the presence of carbon has previously been reported to increase the number of oxygen vacancies in the sample[55], again possibly explaining a change in baseline resistance of the sensor and response due the presence of the SWNTs.

3.6 Selectivity

The enhancements reported upon SWNT inclusion offer a new approach to achieving selectivity in an array of metal-oxide based sensors. Fig.10 demonstrates the selectivity that can be achieved towards EtOH, NH_3, and Acetone with the described modifications to the sensing material. This may be a simpler alternative to doping or temperature modulation of gas sensors currently used to achieve selectivity in real world applications.

4 Conclusion

Novel, printable SWNT-metal oxide inks were synthesised. The composite material displayed an improvement in sensitivity to target vapours when compared to plain WO_3 and SnO_2 semiconducting gas sensors. A 100% increase in sensing response to NO_2 was observed in the sensitivity of the SWNT - WO_3 modified sensor. A similar increase was found in the SWNT- SnO_2 sensor response to Acetone.

The enhancements to both oxidising and reducing gases were found to be dependent on the sensor operating temperature. The composite devices achieved superior sensitivities at

lower temperatures (250 °C), whilst at higher operating temperatures (300 °C) a reduced response magnitude was found for the SWNT modified sensors when compared with the plain metal oxide analogues testing to EtOH and Acetone.

It is suggested that the enhancements observed are a result of (1) the introduction of p-type SWNTs, forming p-n boundaries throughout the composite material and (2) an increase in interaction area due to the presence of SWNT bundles on the sensor surface.

The prolonged sensor recovery times, signal drift and small response magnitudes associated with room temperature SWNT gas sensors were not observed in the elevated temperature SWNT-metal oxide devices, suggesting that nanotube-metal oxide composites may offer a route to improve upon these undesirable characteristics for arrays operating at lower temperatures.

The ability to tailor gas sensor responses through addition of SWNTs would be a useful tool. To introduce a higher degree of discrimination between target gases in a sensor array, sensors are often operated at different temperatures or fabricated from different metal oxides. This work indicates that SWNT inclusion may offer a simpler alternative to achieve selective detection in such an array, via a facile fabrication route.

Acknowledgements

The author thanks E. Newton, A. Naik and D.Williams for their time and useful discussion. S. Firth and K. Reeves are thanked for instrumentation assistance. This work was carried out under EPSRC Grant no: EP/G037264/1 as part of UCL's Security Science Doctoral Training Centre.

Supplementary Information

Additional Raman spectroscopy and XRD data is available for the materials used in synthesis and at various stages of the of the SWNT - metal oxide composite fabrication and testing process. TGA data is supplied to show the mass change of HiPco SWNT material, metal oxides, the ESL Vehicle and the composite material as a function of temperature up to 800°C. Further gas sensor testing results demonstrate the reproducibility of sensor responses after a cycle of testing at higher and lower operating temperatures, along with tests at varying humidity.

References

1 D. Kohl, *Journal of Physics D: Applied Physics*, 2001, **34**, R125.
2 G. F. Fine, L. M. Cavanagh, A. Afonja and R. Binions, *Sensors*, 2010, **10**, 5469–5502.
3 J. Gardner and J. Yinon, *Electronic Noses and Sensors for the Detection of Explosives*, Springer, 2004.
4 B. Timmer, W. Olthuis and A. v. d. Berg, *Sensors and Actuators B: Chemical*, 2005, **107**, 666–677.
5 N. Yamazoe and N. Miura, *Sensors and Actuators B: Chemical*, 1994, **20**, 95–102.
6 W. J. Peveler, R. Binions, S. M. V. Hailes and I. P. Parkin, *Journal of Materials Chemistry A*, 2013, **1**, 2613–2620.
7 J. S. Caygill, F. Davis and S. P. Higson, *Talanta*, 2012, **88**, 14–29.
8 J. Andzelm, N. Govind and A. Maiti, *Chemical physics letters*, 2006, **421**, 58–62.
9 A. Goldoni, L. Petaccia, S. Lizzit and R. Larciprete, *Journal of Physics: Condensed Matter*, 2010, **22**, 013001.
10 P. Teerapanich, M. T. Z. Myint, C. M. Joseph, G. L. Hornyak and J. Dutta, *Transactions on Nanotechnology*, 2013, **12**, 255–262.
11 J. Li and Y. Lu, *ECS Transactions*, 2009, **19**, 7–15.
12 J. M. Schnorr, D. van der Zwaag, J. J. Walish, Y. Weizmann and T. M. Swager, *Advanced Functional Materials*, 2013, n/a–n/a.
13 T. Zhang, S. Mubeen, N. V. Myung and M. A. Deshusses, *Nanotechnology*, 2008, **19**, 332001.
14 J. Li, Y. Lu, Q. Ye, M. Cinke, J. Han and M. Meyyappan, *Nano Letters*, 2003, **3**, 929–933.
15 D. E. Williams, *Sensors and Actuators B: Chemical*, 1999, **57**, 1–16.
16 R. Binions, H. Davies, A. Afonja, S. Dungey, D. Lewis, D. E. Williams and I. P. Parkin, *Journal of The Electrochemical Society*, 2009, **156**, J46–J51.
17 E. J. N. a. S. H. I. P. P. Tarttelin Hernndeza, A. J. T. Naik, *Journal of Materials Chemistry A*, 2014.
18 A. J. T. N. S. M. V. H. a. I. P. P. D. C. Pugh, E. J. Newton, *Journal of Materials Chemistry A*, 2014, 4758–4764.
19 L. Dong, Z. L. Cui and Z. K. Zhang, *Nanostructured materials*, 1997, **8**, 815–823.
20 Y. Zhang, S. Cui, J. Chang, L. E. Ocola and J. Chen, *Nanotechnology*, 2013, **24**, 025503.
21 A. Safavi, N. Maleki and M. M. Doroodmand, *Journal of Experimental Nanoscience*, 2013, **8**, 553–566.
22 W.-Q. Han and A. Zettl, *Nano Letters*, 2003, **3**, 681–683.
23 D. Eder, *Chemical Reviews*, 2010, **110**, 1348–1385.
24 H. Chu, L. Wei, R. Cui, J. Wang and Y. Li, *Coordination Chemistry Reviews*, 2010, **254**, 1117–1134.
25 C. Wongchoosuk, A. Wisitsoraat, A. Tuantranont and T. Kerdcharoen, *Sensors and Actuators B: Chemical*, 2010, **147**, 392–399.
26 P. Nikolaev, M. J. Bronikowski, R. K. Bradley, F. Rohmund, D. T. Colbert, K. A. Smith and R. E. Smalley, *Chemical physics letters*, 1999, **313**, 91–97.
27 I. W. Chiang, B. E. Brinson, A. Y. Huang, P. A. Willis, M. J. Bronikowski, J. L. Margrave, R. E. Smalley and R. H. Hauge, *The Journal of Physical Chemistry B*, 2001, **105**, 8297–8301.
28 W. Wenseleers, I. I. Vlasov, E. Goovaerts, E. D. Obraztsova, A. S. Lobach and A. Bouwen, *Advanced Functional Materials*, 2004, **14**, 1105–1112.
29 J. Zhang, H. Zou, Q. Qing, Y. Yang, Q. Li, Z. Liu, X. Guo and Z. Du, *The Journal of Physical Chemistry B*, 2003, **107**, 3712–3718.
30 A. M. Rao, E. Richter, S. Bandow, B. Chase, P. C. Eklund, K. A. Williams, S. Fang, K. R. Subbaswamy, M. Menon and A. Thess, *Science*, 1997, **275**, 187–191.
31 M. S. Dresselhaus, G. Dresselhaus, R. Saito and A. Jorio, *Physics Reports*, 2005, **409**, 47–99.
32 A. Jorio, R. Saito, J. H. Hafner, C. M. Lieber, M. Hunter, T. McClure, G. Dresselhaus and M. S. Dresselhaus, *Physical Review Letters*, 2001, **86**, 1118.
33 A. R. Harutyunyan, B. K. Pradhan, J. Chang, G. Chen and P. C. Eklund, *The Journal of Physical Chemistry B*, 2002, **106**, 8671–8675.

34 M. Yudasaka, H. Kataura, T. Ichihashi, L.-C. Qin, S. Kar and S. Iijima, *Nano Letters*, 2001, **1**, 487–489.

35 D. E. Williams and K. F. Pratt, *Sensors and Actuators B: Chemical*, 2000, **70**, 214–221.

36 V. Y. Sukharev, *Journal of the Chemical Society, Faraday Transactions*, 1993, **89**, 559–572.

37 N. Yamazoe, G. Sakai and K. Shimanoe, *Catalysis Surveys from Asia*, 2003, **7**, 63–75.

38 E. Indrea, E. Bica, E.-J. Popovici, R.-C. Suciu, M. C. Rosu and T.-D. Silipas, *Revue Roumaine de Chimie*, 2011, **56**, 589–593.

39 D. G. Stroppa, L. A. Montoro, A. Beltran, T. G. Conti, R. O. da Silva, J. Andres, E. R. Leite and A. J. Ramirez, *Chemical Communications*, 2011, **47**, 3117–3119.

40 M. S. Dresselhaus, G. Dresselhaus and R. Saito, *Carbon*, 1995, **33**, 883–891.

41 S. A. Hodge, M. K. Bayazit, K. S. Coleman and M. S. P. Shaffer, *Chemical Society Reviews*, 2012, **41**, 4409.

42 N. Nair, M. L. Usrey, W.-J. Kim, R. D. Braatz and M. S. Strano, *Analytical Chemistry*, 2006, **78**, 7689–7696.

43 R. B. Weisman and S. M. Bachilo, *Nano Letters*, 2003, **3**, 1235–1238.

44 G. Korotcenkov, *Materials Science and Engineering: B*, 2007, **139**, 1–23.

45 H.-Q. Nguyen and J.-S. Huh, *Sensors and Actuators B: Chemical*, 2006, **117**, 426–430.

46 C. Cantalini, L. Valentini, L. Lozzi, I. Armentano, J. M. Kenny and S. Santucci, *Sensors and Actuators B: Chemical*, 2003, **93**, 333–337.

47 M. DArienzo, D. Cristofori, R. Scotti and F. Morazzoni, *Chemistry of Materials*, 2013, **25**, 3675–3686.

48 D. S. Vlachos, P. D. Skafidas and J. N. Avaritsiotis, *Sensors and Actuators B: Chemical*, 1995, **25**, 491–494.

49 J. F. McAleer, P. T. Moseley, J. O. W. Norris and D. E. Williams, *Journal of the Chemical Society, Faraday Transactions 1: Physical Chemistry in Condensed Phases*, 1987, **83**, 1323–1346.

50 J. F. McAleer, P. T. Moseley, J. O. W. Norris, D. E. Williams and B. C. Tofield, *Journal of the Chemical Society, Faraday Transactions 1: Physical Chemistry in Condensed Phases*, 1988, **84**, 441–457.

51 J. F. McAleer, A. Maignan, P. T. Moseley and D. E. Williams, *Journal of the Chemical Society, Faraday Transactions 1: Physical Chemistry in Condensed Phases*, 1989, **85**, 783–799.

52 G. Chabanis, I. P. Parkin and D. E. Williams, *Measurement Science and Technology*, 2003, **14**, 76.

53 S. Mubeen, M. Lai, T. Zhang, J.-H. Lim, A. Mulchandani, M. A. Deshusses and N. V. Myung, *Electrochimica Acta*, 2013, **92**, 484–490.

54 N. Van Hieu, L. T. B. Thuy and N. D. Chien, *Sensors and Actuators B: Chemical*, 2008, **129**, 888–895.

55 M. Epifani, J. D. Prades, E. Comini, E. Pellicer, M. Avella, P. Siciliano, G. Faglia, A. Cirera, R. Scotti, F. Morazzoni and J. R. Morante, *The Journal of Physical Chemistry C*, 2008, **112**, 19540–19546.

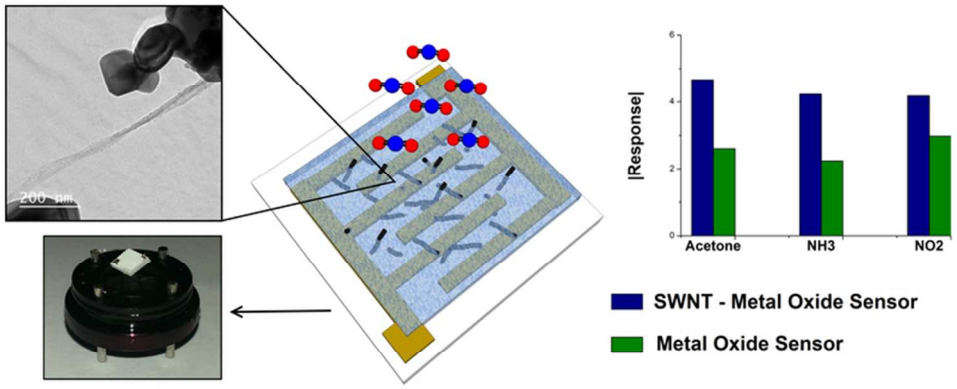

35x15mm (600 x 600 DPI)

,SWNT – metal oxide composites for improvement of response and selectivity in gas sensors.